2016-07

Intraseasonal Cross-Shelf Variability of Hypoxia along the Newport, Oregon, Hydrographic Line

Adams, KA

10.1175/JPO-D-15-0119.1
JOURNAL OF PHYSICAL OCEANOGRAPHY

Intraseasonal Cross-Shelf Variability of Hypoxia along the Newport, Oregon, Hydrographic Line

KATHERINE A. ADAMS

School of Marine Science and Engineering, Plymouth University, Plymouth, United Kingdom

JOHN A. BARTH AND R. KIPP SHEARMAN

College of Earth, Ocean and Atmospheric Sciences, Oregon State University, Corvallis, Oregon

(Manuscript received 7 July 2015, in final form 15 April 2016)

ABSTRACT

Observations of hypoxia, dissolved oxygen (DO) concentrations $< 1.4\,\text{ml}\,\text{L}^{-1}$, off the central Oregon coast vary in duration and spatial extent throughout each upwelling season. Underwater glider measurements along the Newport hydrographic line (NH-Line) reveal cross-shelf DO gradients at a horizontal resolution nearly 30 times greater than previous ship-based station sampling. Two prevalent hypoxic locations are identified along the NH-Line, as is a midshelf region with less severe hypoxia north of Stonewall Bank. Intraseasonal cross-shelf variability is investigated with 10 sequential glider lines and a midshelf mooring time series during the 2011 upwelling season. The cross-sectional area of hypoxia observed in the glider lines ranges from 0 to 1.41 km^2. The vertical extent of hypoxia in the water column agrees well with the bottom mixed layer height. Midshelf mooring water velocities show that cross-shelf advection cannot account for the increase in outer-shelf hypoxia observed in the glider sequence. This change is attributed to an along-shelf DO gradient of $-0.72\,\text{ml}\,\text{L}^{-1}$ over 2.58 km or $0.28\,\text{ml}\,\text{L}^{-1}\,\text{km}^{-1}$. In early July of the 2011 upwelling season, near-bottom cross-shelf currents reverse direction as an onshore flow at 30-m depth is observed. This shoaling of the return flow depth throughout the season, as the equatorward coastal jet moves offshore, results in a more retentive near-bottom environment more vulnerable to hypoxia. Slope Burger numbers calculated across the season do not reconcile this return flow depth change, providing evidence that simplified two-dimensional upwelling model assumptions do not hold in this location.

1. Introduction

Subsurface waters low in dissolved oxygen (DO) upwell onto the continental shelf along the U.S. West Coast each spring and summer. As wind-driven coastal upwelling seasons progress, near-bottom DO concentrations below the hypoxic threshold ($1.4\,\text{ml}\,\text{L}^{-1}$) are observed off Washington, Oregon, and California. These so-called dead zones (Diaz and Rosenberg 2008) are not linked to anthropogenic eutrophication like the majority of coastal and estuarine low DO environments on the southern and eastern coasts of the United States but have similar detrimental effects on marine organisms (Diaz and Rosenberg 1995; Gray et al. 2002; Keller et al. 2010). Off central Oregon, hypoxia has been observed across the shelf and throughout the upwelling season, with ~3 months of persistent, seasonal hypoxia in one location (Adams et al. 2013), yet invertebrate and fish kills are only occasionally observed (Grantham et al. 2004; Chan et al. 2008). The severity and duration of low DO events vary in both space and time, yet extant datasets have not resolved cross-shelf and along-shelf gradients $O(<10)$ km on intraseasonal (15–40 day) time scales.

Spatial and temporal variability of hypoxia has been observed on decadal, interannual, intraseasonal, event, and tidal scales (Adams et al. 2013; Peterson et al. 2013; Pierce et al. 2012, Chan et al. 2008; Hales et al. 2006; Grantham et al. 2004); however, previous studies consisted of few high-resolution or several low-resolution realizations, forsaking either temporal or spatial resolution for the other. Underwater gliders with nonstop data collection allow investigations of cross-shelf variability on finer temporal and spatial scales than previous

Corresponding author address: Katherine Adams, School of Marine Science and Engineering, Plymouth University, Drake Circus, Plymouth, PL4 8AA United Kingdom.
E-mail: kate.adams@plymouth.ac.uk

DOI: 10.1175/JPO-D-15-0119.1

ship-based CTD station surveys along the Newport hydrographic line (NH-Line; 44.65°N).

Seasonal DO decline on the central Oregon midshelf, 70- to 80-m isobaths, has been calculated from ship-based observations (Hales et al. 2006) and from moored continuous time series (Adams et al. 2013). Both studies have reported a local seasonal decline rate of $\sim 0.01\,\mathrm{ml\,L^{-1}\,day^{-1}}$. This decline is the result of local respiration balanced by physical advection and mixing processes. Adams et al. (2013) calculate the local rate of change as only ⅓ of the expected local respiration drawdown on the shelf and find physical processes keep the system from reaching anoxia. In a shelf DO flux budget, Hales et al. (2006) find physical advection mechanisms to be of the same magnitude as the local rate of change. However, this budget was calculated from four cross-shelf sections separated by 2 months in time and ~40 km in along-shelf distance. This yields early and late-season snapshots but does not resolve intraseasonal variability. Hypoxic waters off central Oregon develop and evolve throughout each season, influenced by physical and biological processes in concert, all with along-shelf and cross-shelf gradients that have not been well resolved to date.

An important detail not addressed in the current California Current System (CCS) near-bottom DO variability literature is the intraseasonal variability of near-bottom flow. The onshore return flow depth during upwelling can occur in the bottom boundary layer (BBL) or in the interior of the water column (Huyer et al. 1979; Smith 1981). The return flow depth has previously been related to the slope Burger number S, which depends on the water column stratification, Coriolis parameter and bottom slope. An S value of ~1 indicates a return flow in the interior for the Oregon coast (Lentz and Chapman 2004). The BBL flow may also diminish from buoyancy arrest (Garrett et al. 1993) where onshore transport in the bottom stalls. Evidence that an onshore interior flow depth varying with the mean along-shelf pressure gradient has been reported in the northern CCS (McCabe et al. 2015). Regardless of the mechanism, return flow depth is important to DO dynamics on the shelf since near-bottom waters rely on cross-shelf currents for flushing and replenishment with source water. As the propensity of hypoxic observations is at near-bottom depths, BBL flows are paramount to identifying the effect of physical advection mechanisms on near-bottom DO dynamics.

Here, we first use a combination of mooring and glider data to resolve finescale DO variability spatially (<1 km) and temporally (days–months) and then test hypothetical mechanisms responsible for the observed variability. Data sources and processing methods are detailed in section 2. Midshelf mooring and glider data are presented for the 2011 upwelling season in section 3a. Spatial patterns of glider-measured hypoxia are determined in section 3b. The importance of cross-shelf and along-shelf circulation and return flow depth on hypoxia is discussed in section 4. Finally, we summarize and conclude our findings in section 5.

2. Data and methods

a. Data

1) Newport hydrographic line glider data 2006–12

The continental shelf and slope waters along the historic Newport hydrographic line (44.65°N) were sampled by Teledyne Webb Electric G1 Slocum gliders (0- to 200-m water depth; 124.1°W to 125.1°W; 2006 to 2012) operated by the Oregon State University (OSU) glider group. The Slocum gliders sampled from 2 to 90 km offshore with cross-shelf transects taking an average of 3.8 ± 1.1 days. With a pitch angle of approximately 26°, the maximum horizontal separation of Slocum glider vertical dive and climb pairs ranges from 62 to 410 m for 30- and 200-m water depths, respectively. Variability in the glider's location during cross-shelf transects arises from the slow horizontal vehicle speed, $0.25\,\mathrm{m\,s^{-1}}$, compared with the strong along-shelf coastal currents: 0.5–1 $\mathrm{m\,s^{-1}}$ coastal upwelling jet and 1–2 $\mathrm{m\,s^{-1}}$ wintertime Davidson Current.

Slocum gliders collected data via a Sea-Bird Electronics, Inc. (SBE), 41CP unpumped CTD measuring conductivity, temperature, and pressure and an Aanderaa 3835 optode measuring dissolved oxygen. Thermal–mass corrections to the conductivity cell have been applied for the Slocum glider dataset prior to oxygen concentration calculations (Garau et al. 2011). The dissolved oxygen dataset is shifted by the reported 24-s response time of the optode.

2) Optode calibration procedure

Dissolved oxygen optode sensors aboard the Slocum gliders were calibrated in the laboratory several times each year of operation. The two-point linear calibration procedure consisted of triplicate Winkler titration samples taken at a midrange (5–6 $\mathrm{ml\,L^{-1}}$) concentration followed by the addition of sodium sulfite to a glass, well-stirred container until a zero point for each sensor is reached. The slopes and offsets calculated after each in-laboratory calibration are applied to the measured DO values. In-laboratory calibrations were conducted approximately quarterly and after each manufacturer factory service.

3) GLIDER-CALCULATED DEPTH-AVERAGED CURRENTS

Depth-averaged currents are inferred by Slocum gliders by dead reckoning (e.g., Merckelbach et al. 2008). Using the glider vehicle flight model, the glider's target location in still water is calculated. The difference between the target location and the actual location during the next GPS reading per travel time is the dive-averaged current for the top 200 m of the water column, which has a north (N)–south (S) component v_{avg}. Glider v_{avg} values are calculated between glider GPS readings. The time between GPS readings, 1 to 6 h, is user defined and varies with distance offshore. Around the midshelf (80-m isobath), one dive–climb pair takes approximately 1 h, and the ''callback interval'' is typically set to 3 h. Thus, each midshelf v_{avg} calculation applies to six vertical profiles.

Reported accuracies of glider-calculated, depth-averaged currents are $O(0.01)$ m s^{-1} in glider studies in deeper waters using the Seaglider and Spray gliders (Eriksen et al. 2001; Todd et al. 2011) that calculate the depth-averaged current after each dive–climb pair. Inaccuracies $O(0.05)$ m s^{-1} have been reported for Slocum-measured v_{avg} values due to compass calibration error and from the exclusion of attack angle in the Slocum flight model (Ordonez 2012; Merckelbach et al. 2008). This error should also be attributed to the dynamic environments Slocum gliders are used in and the length of time between the v_{avg} calculations. A comparison of moored and glider-derived N–S velocities over the midshelf is presented in the appendix.

4) NH-LINE MIDSHELF MOORING (NH10)

Horizontal water velocity, temperature, conductivity, and dissolved oxygen data from the 2011 upwelling season are analyzed from the NH-10 buoy (44.65°N, 124.30°W, 80-m water depth, 18-km offshore) along the NH-Line. A downward-looking Teledyne RD Instruments 300-kHz Workhorse Sentinel measured horizontal water column velocities at 7–73-m depths in 2-min intervals and 2-m bins. N–S and east (E)–west (W) velocities are corrected for magnetic declination and subsequently rotated into principal axes (22.3° true) based on depth average velocities from the 2011 upwelling season deployment. This rotation minimizes variability in the cross-shelf direction and is similar to the orientation of local isobaths. Rotated E–W and N–S velocities are referred to hereinafter as cross-shelf and along-shelf velocities, respectively.

Temperature and conductivity data were measured by a SBE16plus at 73-m depth and a SBE16 at 60-m depth. SBE-reported accuracies for the temperature and conductivity sensors are 0.002°C and 0.002 (equivalent salinity), respectively. A Clark electrode-type SBE43 was installed on both instruments for dissolved oxygen measurements. Temperature, salinity, and dissolved oxygen data, recorded at 2-h intervals, were 40-h low-pass filtered. The 73-m time series is incomplete due to instrument failure. Sensors on the 73- and 60-m instruments were factory calibrated prior to the April 2011 and 2010 deployments, respectively.

5) STRAWBERRY HILL MIDSHELF MOORING (SH70)

In 2011, near-bottom temperature, conductivity, DO, and current data were collected on the 70-m isobath approximately 40 km to the south of the NH-Line (Fig. 1) off Strawberry Hill (SH70; 44.25°N, 124.25°W), previously presented in Adams et al. (2013). SBE16plus CTD and SBE43 DO sensors collected measurements on 30-min intervals. Current measurements made using a Teledyne RD Instruments 300-kHz Workhorse Sentinel ADCP were filtered and rotated similar to NH10 currents described above. CTD and DO sensors were factory calibrated before and after each field season. Several in-laboratory and calibration casts were taken throughout the season to verify the CTD and DO data quality.

6) WIND STRESS

Wind speed and direction were measured at 10-min intervals at National Data Buoy Center (NDBC) station 46050 (44.64°N, 124.53°W; 35-km offshore). Wind measurements at station 46050 correlate strongly with those from the coastal meteorological station (NWP03; 44.61°N, 124.07°W), with a correlation coefficient of 0.76 at zero lag. Gaps in the 2011 station 46050 record were filled with NWP03 winds using the regression coefficients: slope 0.90, offset 0.34 m s^{-1}. The N–S wind stress was derived (Large et al. 1994) from hourly averaged wind speed and direction prior to 40-h low-pass filtering to remove high-frequency variability, for example, diurnal sea breeze, which is not a focus of this study.

b. Derived data product methods

1) GLIDER DATA GRIDDING AND FILTERING

The Slocum datasets were binned by depth (2 m) and gridded using two methods. Linear interpolation resulted in unfiltered gridded glider lines on a desired grid. Filtered, gridded glider lines were processed using an iterative two-dimensional Gaussian function (Barnes 1964) with decorrelation radii of 10 km in the horizontal and 5 m in the vertical. These smoothing length scales were determined from spatial autocorrelations and power

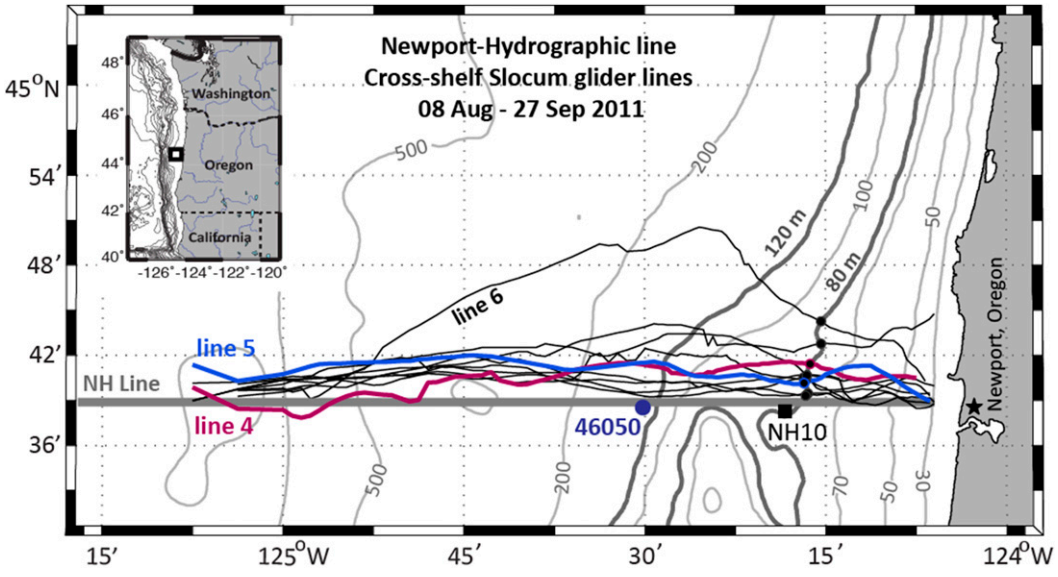

FIG. 1. Central Oregon coast study map with glider tracks along the NH-Line from 10 sequential Slocum glider cross-shelf transects from late summer 2011. Glider lines span 2–90 km offshore (124.1°–125.1°W). Mooring locations (black squares) are shown for the NH-Line midshelf (NH10; 80-m water depth) and Strawberry Hill line midshelf (SH70; 70-m water depth). Wind data were measured at NDBC buoy 46050 and at a coastal meteorological station (NWP03). The midshelf (80 m) and outer-shelf (120 m) isobaths are shown in bold. Black circles on the 80-m isobath indicate the locations of glider 80-m isobath crossings.

spectral density behavior of isopycnal depths along each cross-shelf transect. Previous glider studies within the CCS found horizontal smoothing scales of 25–30 km were necessary to remove high-frequency signals such as internal waves [University of Washington (UW) Seagliders in Pelland et al. (2013); Spray gliders in Todd et al. (2011) and Rudnick and Cole (2011)]. The specified grid is the same for both methods and telescopes horizontally and vertically due to the depth-dependent separation distances of glider dive and climb pairs. The grid resolution over the shelf and shelf break, 500 m and 1 km, assures multiple measurements per grid cell. Therefore, the resolution of the gridded data presented here allows for an analysis of cross-shelf features, $O(1)$ km in size, an order of magnitude increase from the 5-nm (9.3 km) historical NH-Line station spacing. A regular grid would have been used if the glider lines did not sample the continental shelf. Unfiltered glider lines are used to analyze scalars, that is, DO. Filtered glider lines are used prior to calculations such as geostrophic velocity (see below). Filtering of glider-calculated v_{avg} was necessary to remove tidal frequency aliasing; the Barnes (1964) algorithm was used with a horizontal decorrelation radius of 10 km.

2) GLIDER-DERIVED GEOSTROPHIC AND ABSOLUTE N–S VELOCITIES

The N–S geostrophic velocities are calculated from gridded and filtered cross-shelf glider temperature and salinity sections (not shown). Each horizontal grid space represents a different sampling station, analogous to tightly spaced, ship-based CTD observations. The reference level, or level of no motion, is set to 190 m. Geopotential anomaly is calculated by vertically integrating specific anomaly changes with depth, starting from zero at the reference level for each horizontal station. For stations where the bottom depth is less than the reference level, geopotential anomaly at the deepest data point for each station is linearly extrapolated from the two nearest offshore stations following Reid and Mantyla (1976). Specific volume anomaly is then vertically integrated from this extrapolated value rather than from zero at the reference level. This method assumes zero horizontal shear in geostrophic velocity between the stations at their deepest common depth.

Cross-path geostrophic velocities are then calculated by taking the horizontal difference between geopotential anomalies of two adjacent horizontal stations and dividing by the Coriolis parameter and the horizontal distance between stations. Geostrophic velocity vectors are orthogonal to glider paths that deviate from a line of constant latitude. Hence, only the N–S component of the calculated geostrophic velocity vector is retained: v_{geo}.

An absolute N–S velocity can be obtained from v_{geo} by adding the N–S component of glider-calculated depth-averaged velocity v_{avg} to v_{geo}, similar to Todd

et al. (2009). Comparison of depth-averaged and 70-m depth moored N–S velocities in the appendix shows a $+0.05\,\mathrm{m\,s^{-1}}$ offset of v_{abs} over the 80-m isobath. Corrections of N–S depth-averaged velocities calculated from measured compass inaccuracies after the 2011 Slocum glider deployments are on the order of $0.03\,\mathrm{m\,s^{-1}}$.

3. Results

Variability of cross-shelf, near-bottom DO concentrations on intraseasonal time scales (weekly–monthly) are investigated using 10 sequential Slocum cross-shelf sections of the NH-Line (44.65°N) sampled over 50 days (8 August–27 September 2011; Fig. 1). Glider lines took 3–7.5 days to sample from 124.1° to 125.1°W (2–90 km from shore), spanning from the 30- to the 1500-m isobath (Table 1). The duration of each line depended on the strength and directionality of coastal water velocities. Moored continuous time series from two midshelf moorings, NH10 and SH70 (Fig. 1), are included in the analysis to 1) provide context to the glider sequence collected late in the 2011 upwelling season and 2) investigate intraseasonal variability of near-bottom currents potentially important for near-bottom DO variability.

a. 2011 midshelf mooring and glider time series

Central Oregon coastal winds shifted to upwelling favorable around yearday 106 (15 April) (Pierce et al. 2006; http://damp.coas.oregonstate.edu), although the cold, salty, and low DO signature of upwelling source water was not observed until early May (yearday 128; 7 May; Adams et al. 2013). The N–S wind stress (Fig. 2a) shows predominantly upwelling-favorable wind forcing until mid-September when a strong poleward wind event was observed. Relaxations and reversals of upwelling-favorable winds are infrequent late in the upwelling season, July–September, compared to earlier in the season.

Continuous time series of near-bottom density σ_θ and DO from the midshelf moorings NH10 (73-m measurements in 80-m water depth) and SH70 (70-m water depth) are presented in Figs. 2b and 2c. Data from the NH10 60-m DO sensor are also included, since the 73-m DO sensor failed during the deployment. The time series show a density increase to $26.5\,\mathrm{kg\,m^{-3}}$ and a gradual DO decrease throughout the upwelling season. Moored DO at NH10 (73 and 60 m) approaches the hypoxic threshold ($1.4\,\mathrm{ml\,L^{-1}}$) several times throughout the time series, but persistent hypoxia is not observed until early August (Fig. 2c). The SH70 DO record, however, is persistently hypoxic for over 100 days. This location has

TABLE 1. 2011 Sequential Slocum glider cross-shelf section information. Times (UTC) at inshore (NH1; 124.1°W) and offshore (NH45; 125.1°W) turnaround points as well as times crossing the 80-m isobath area. Hypoxic area and height are calculated from unfiltered gridded oxygen data. Hypoxic area is calculated by integrating the cross-shelf and vertical extent of the hypoxic measurements in each unfiltered, gridded glider line. Hypoxic height is the distance from the shelf bottom to the hypoxic oxycline (Fig. 4). BML height at the 80-m isobath, also reported in mab, requires a density difference of $0.02\,\mathrm{kg\,m^{-3}}$ between consecutive vertical bins. BBL cross-shelf Ekman transport calculations from NH10 moored ADCP data.

Glider line no.	Inshore time (calendar day/yearday)	Offshore time (calendar day/yearday)	Duration (days)	80-m isobath (calendar day/yearday)	Hypoxic area ($\mathrm{km^2}$)	Median hypoxic height (mab)	Hypoxic height 80 m (mab)	BML height 80 m (mab)	U_b^{EK} 80 m ($\mathrm{m^2\,s^{-1}}$)
1	8 Aug 0016:01/221.01	11 Aug 0244:36/224.11	3.10	08 Aug 1930:08/221.81	0	N/A	N/A	15	−0.35
2	16 Aug 1322:41/229.56	11 Aug 0625:53/224.27	5.29	15 Aug 0450:26/228.20	0.30	15 ± 7	5	15	−0.51
3	16 Aug 1715:11/229.72	19 Aug 2007:20/232.84	3.12	17 Aug 1503:53/230.63	0.49	15 ± 7	20	15	0.32
4	25 Aug 2008:55/238.84	20 Aug 0241:36/233.11	5.72	25 Aug 0312:15/238.13	0.38	15 ± 6	20	10	0.13
5	25 Aug 2037:58/238.86	28 Aug 1936:10/241.82	2.96	26 Aug 1801:23/239.75	0.85	25 ± 8	25	25	0.88
6	5 Sep 1016:31/249.43	29 Aug 0011:33/242.01	7.42	04 Sep 1459:37/248.62	1.05	30 ± 8	40	25	−1.00
7	5 Sep 1056:57/249.46	08 Sep 1334:47/252.57	3.11	6 Sep 0631:47/250.27	1.41	25 ± 16	10	15	0.81
8	13 Sep 0143:28/257.07	08 Sep 1425:19/252.60	4.47	11 Sep 2324:23/255.98	1.16	25 ± 16	15	10	−1.29
9	19 Sep 1902:54/263.79	22 Sep 1805:37/266.75	2.96	20 Sep 1534:09/264.65	0.50	15 ± 9	5	10	−0.58
10	27 Sep 1939:54/267.32	23 Sep 0734:56/271.82	4.50	26 Sep 2000:44/270.83	0.66	25 ± 17	5	20	−0.49

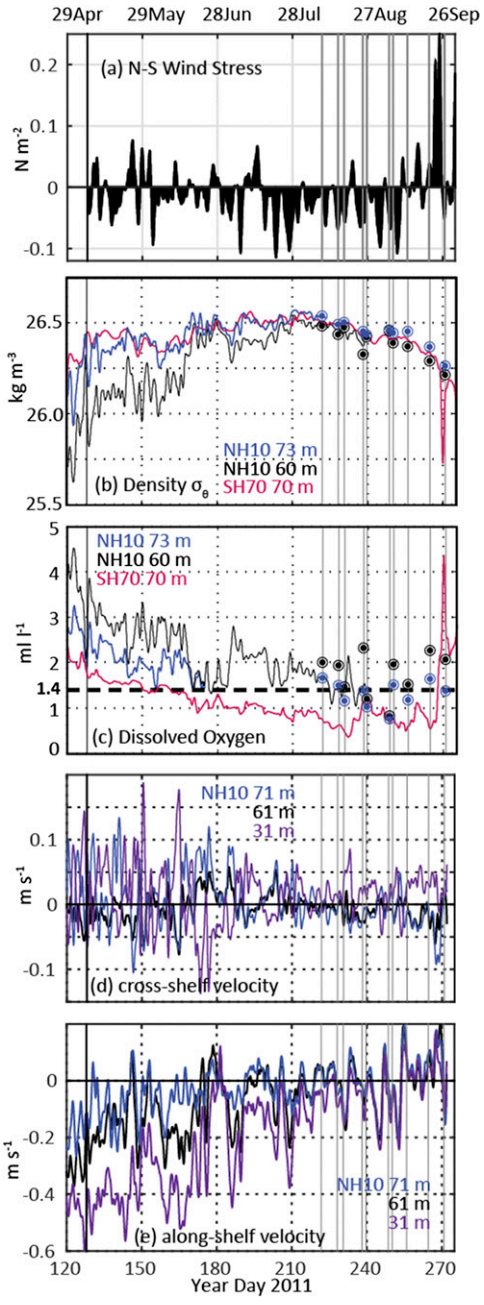

FIG. 2. (a) 2011 upwelling season N–S wind stress (N m^{-2}) from NDBC buoy46050 wind data. Midshelf mooring continuous time series from NH10 (44.65°N, 124.3°W; 80-m water depth) and SH70 (44.25°N, 124.25°W; 70-m water depth) of (b) potential density anomaly (kg m^{-3}), (c) dissolved oxygen (ml L^{-1}), (d) cross-shelf velocity–depth average, and (e) along-shelf velocities at several ADCP depth bins for NH10 and the near-bottom bin for SH70. Positive velocities are onshore and poleward, respectively. The circles in (b) and (c) correspond to 70- (blue) and 60-m (black) Slocum glider data at each 80-m isobath crossing in glider sections 1–10 (gray lines; Fig. 1). A solid black line at 7 May marks the 2011 spring transition, or beginning of the upwelling season, as found in Adams et al. (2013).

previously been identified as vulnerable to hypoxia due to high productivity, recirculation of currents, and low flushing rates over the bank (Barth et al. 2005; Castelao and Barth 2005; Adams et al. 2013). A similar seasonal DO decline rate is observed in both the NH10 and SH70 near-bottom DO time series [$\sim$1 ml L^{-1} (100 days)$^{-1}$; Adams et al. 2013].

Unfiltered gridded glider data from the 10 sequential glider lines (Fig. 1) from 60- and 70-m water depths at each 80-m isobath crossing are plotted alongside the moored density and DO time series (Figs. 2b,c). During the short overlapping section with the moored continuous time series, there is good agreement between glider and mooring data. Late-season glider-measured density steadily decreases from 26.5 to 26.25 kg m^{-3} at 70 m (Figs. 2a,b), while a trend in near-bottom DO is less clear. The scatter of glider-measured DO (Fig. 2c) is expected since the separation of measurements at the 80-m isobath ranges from 2.6 to 9.8 days (Table 2). There is also latitudinal variability in the 80-m isobath crossings (Fig. 1).

Cross-shelf and along-shelf velocities from the NH10 mooring are presented at 31-, 61- and 71-m depth bins (Figs. 2d,e). At the deepest bin, 71 m, positive (onshore) flow is seen early in the upwelling season but decreases in magnitude later in the season. At a shallower depth bin, 31 m, positive (onshore) flow is observed throughout most of the upwelling season. Although the magnitude of the flow decreases late in the season, flow at 31 m remains onshore. Onshore interior flow is also observed by McCabe et al. (2015) on the Washington shelf late in the upwelling season of 2005.

Along-shelf velocities are negative (equatorward) and decrease with time from late April to late July at all depths. This is consistent with the equatorward coastal jet moving farther offshore later in the upwelling season (Barth et al. 2005). Although not a focus of this paper, event-scale variability (2–5 days) is observed in all fields in Fig. 2.

Trends of measured quantities during the 2011 upwelling season are shown in Fig. 3. Cumulative wind stress (Fig. 3a) shows persistent upwelling-favorable wind conditions throughout the upwelling season until September. Time-integrated currents, or cumulative displacements (CD), clearly show abrupt changes to flow magnitude and direction. The positive slope of cross-shelf CD (Fig. 3b) at 73 m early in the season (days 120–200) indicate strong onshore flow near the bottom. A transition to a negative slope around day 210 is indicative of weak and offshore near-bottom currents at the 80-m isobaths. At SH70, onshore currents are near zero until midseason. The slopes of all along-shelf CD (Fig. 3c) are negative and weaken

TABLE 2. Change in observed DO10 m above the bottom at the 80- and 120-m isobaths from glider-measured DO (Fig. 6a). Discrete observed DO rates of change (Δ DO per Δ time) are calculated. Estimates for density-driven (Δ 0.32 ml L^{-1} per Δ 0.1 kg m^{-3}) and biologically driven (2.6×10^{-2} ml L^{-1} day^{-1}) DO rates of change are calculated based on Adams et al. (2013). Observed DO decline rates are bold if larger than 2.6×10^{-2} ml L^{-1} day^{-1}.

Glider lines	Δ time 80-m isobath (days)	Observed Δ DO 70/80 m (ml L^{-1})	Observed Δ DO rate 70/80 m (10^{-2} ml L^{-1} day^{-1})	Estimated Density Δ DO 70/80 m (ml L^{-1})	Estimated Biological Δ DO 70/80 m (ml L^{-1})
2–1	6.4	−0.16	**−3.02**	0.15	−0.17
3–2	2.4	−0.34	**−9.44**	−0.03	−0.06
4–3	7.5	0.22	3.49	0.16	−0.20
5–4	1.5	−0.35	**−12.50**	0.06	−0.04
6–5	8.9	−0.27	**−3.38**	−0.09	−0.23
7–6	1.6	0.75	28.85	0.04	−0.04
8–7	5.7	−0.32	**−6.96**	−0.02	−0.15
9–8	8.7	0.46	4.69	0.27	−0.23
10–9	6.2	−0.26	**−5.42**	0.34	−0.16
	Δ time 120-m isobath (days)	Observed Δ DO 110/120 m (ml L^{-1})	Observed Δ DO rate 110/120 m (10^{-2} ml L^{-1} day^{-1})	Estimated density Δ DO 110/120 m (ml L^{-1})	Estimated biological Δ DO 110/120 m (ml L^{-1})
2–1	5.3	−0.33	**−5.16**	−0.08	−0.14
3–2	3.6	0.24	10.00	0.004	−0.09
4–3	6.3	0.16	2.13	0.13	−0.16
5–4	2.8	−0.72	**−45.00**	0.02	−0.07
6–5	8.0	−0.14	−1.57	−0.07	−0.21
7–6	2.6	0.02	1.25	0.13	−0.07
8–7	4.6	0.06	1.05	0.01	−0.12
9–8	9.8	0.22	2.53	0.13	−0.26
10–9	4.8	0.25	4.03	0.32	−0.13

sharply around day 200, when the coastal jet has moved offshore.

Low CD values at the 61-m depth bin (Figs. 3b,c) indicate overall weak cross-shelf flow at this depth. This weak flow suggests 60 m is the transition from the interior to the bottom mixed layer (BML). This is consistent with ~20-m BML heights from the glider 80-m isobath crossings (Table 1). BML height is defined as the first vertical grid cell from the bottom of each horizontal grid column with a density difference greater than 0.2 kg m^{-3}.

At the shallower 31-m depth bin, the cross-shelf CD slope is strongly positive after day 190 as the near-bottom currents switch to weak and offshore flow (Fig. 3b). This is indicative of onshore return flow in the interior rather than the BBL, observed previously off the coast of Oregon (Huyer 1976) and Washington (McCabe et al. 2015). This has implications for near-bottom flushing rates late in the season and is investigated further in section 3c; also affected are the near-bottom water mass properties that are less dense (Fig. 2b) and warmer (McCabe et al. 2015) late in the season.

A shallow return flow depth below the surface Ekman layer has also been shown using a two-dimensional upwelling model with slope Burger number $S \sim 1$ (Lentz and Chapman 2004). We investigate the relationship between S and return flow depth in section 3d. The temporary sharp change in the 31-m cross-shelf CD slope between days 170 and 190 is due to a deepening of the surface layer offshore flow.

The apparent weakening of the cross-shelf near-bottom flow during the 2011 upwelling season is investigated further. Cross-shelf Ekman BBL transport is calculated using overlying interior water velocities from the formulation

$$U_b^{\mathrm{Ek}} = \frac{\tau_b^y}{\rho_o f} = -\frac{\delta}{2}(u_i + v_i), \tag{1}$$

where the along-shelf bottom stress τ_b^y is related to the cross-shelf and along-shelf interior flows just above the Ekman BBL height δ, here assumed to be 20 and 10 m above the bottom (mab). Using a nominal density of 1026 kg m^{-3} and the time series of moored NH10 ADCP currents at the 61- and 71-m depth bins, U_b^{Ek} is calculated (Fig. 3d). Onshore transport in the BBL is much stronger and persistent at the beginning of the 2011 upwelling season and decreases late in the season at both depths. Toward the end of the upwelling season, U_b^{Ek} alternates from onshore and offshore with much

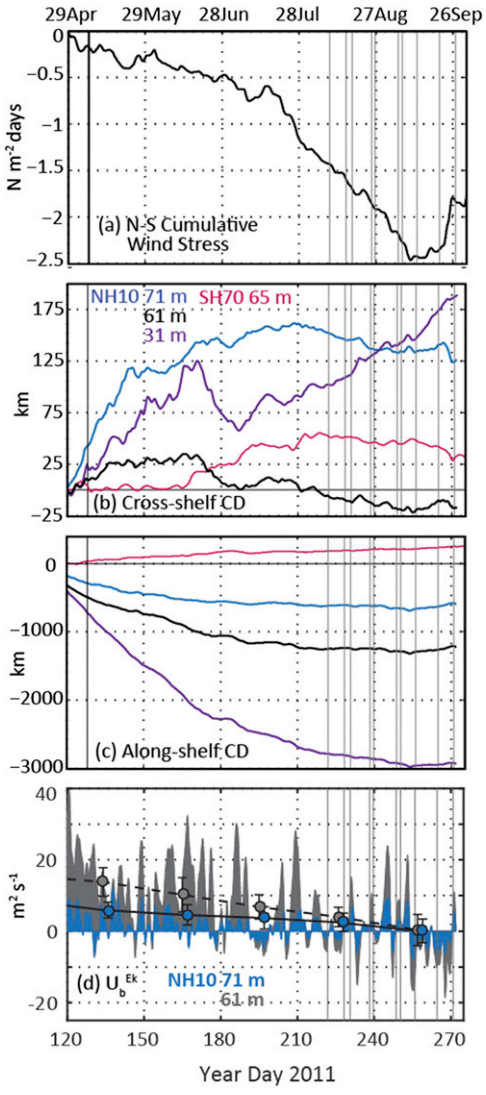

FIG. 3. Time series of (a) cumulative wind stress at NDBC buoy 46050 and time-integrated currents, or cumulative displacements, from the (b) cross-shelf and (c) along-shelf velocities from the NH10 (80-m water depth) and SH70 (70-m water depth) midshelf moorings. Positive CD values are onshore and north, respectively. (d) Bottom Ekman cross-shelf transport ($m^2\,s^{-1}$) at 20 (blue) and 10 mab (gray) calculated from NH10 moored velocities. Monthly means plus or minus one standard deviation of bottom Ekman transport is also plotted at 20 (dashed) and 10 mab.

weaker magnitudes than earlier in the season. The glider lines presented in section 3b were collected late in the upwelling season, hence during a time of weak cross-shelf transport in the BBL. A seasonal decline in U_b^{Ek} is also evident from monthly averages of 2006–12 NH10 ADCP currents, ranging from 15 to $0\,m^2\,s^{-1}$ from April to September at 20 mab (Fig. 3). This is further evidence that late-season flow in the BBL is weak or arrested.

Here, estimates of U_b^{Ek} are calculated, assuming constant BBL heights throughout the upwelling season. Measurements in Perlin et al. (2005) show the importance of event-scale variability and background flow conditions on BBL height. Specifically, the BBL height increases over the bed during poleward near-bottom flow or wind relaxations or downwelling-favorable wind events.

b. 2011 NH-Line glider sequence (8 August–27 September)

1) UNFILTERED DISSOLVED OXYGEN AND DENSITY

Cross-shelf (NH-Line) sections of DO and potential density anomaly σ_θ for the 10 sequential glider lines in late summer 2011 are shown in Fig. 4. The direction of the glider path (onshore or offshore) is indicated by arrows, alternating direction every other line. The shelf bottom topography in line 6 is steeper and narrower than in other sections. As shown in Fig. 1, the glider path during line 6 deviated to the north of the NH-Line (14 km at maximum separation). Tidal-band frequency undulations observed in the high-oxygen, low-density contours (Fig. 4, lines 3–5) can also be seen in near-bottom fields, likely due to the energetic internal M2 tide observed in this region (Suanda and Barth 2015).

DO observations are lowest above the bottom in all sections (Fig. 4). Upwelling source water, or offshore water along isopycnals that upwell on to the shelf, is higher in DO than over the shelf. This follows Adams et al. (2013), which report glider-measured source water DO concentrations, $2.2\,ml\,L^{-1}$ at $26.5\,kg\,m^{-3}$ in 2011, at the offshore station NH25 (Fig. 1) Hence, an onshore near-bottom flow of source water is expected to be a source of DO for the near-bottom environment by flushing and replenishing low DO shelf water (Fig. 2c).

2) HYPOXIA

Near-bottom hypoxia (black contour in Fig. 4a) is observed in each panel except for line 1, with cross-sectional hypoxic areas increasing from $0\,km^2$ in section 1 to $1.41\,km^2$ in line 7. Hypoxia is first observed in line 2 in two distinct locations: over the 60–80-m isobaths and the 120–140-m isobaths. By line 4, hypoxia is observed only upslope of the 80-m isobath. In the next line (5), the hypoxic area extends down to 160 m. In line 6–8, hypoxia is observed down to the full depth range of the Slocum gliders, although the hypoxic area and median hypoxic height above the bottom varies (Table 1). In line 9, hypoxia is again present in two distinct zones as observed in lines 2 and 3. Finally, in line 10, near-bottom

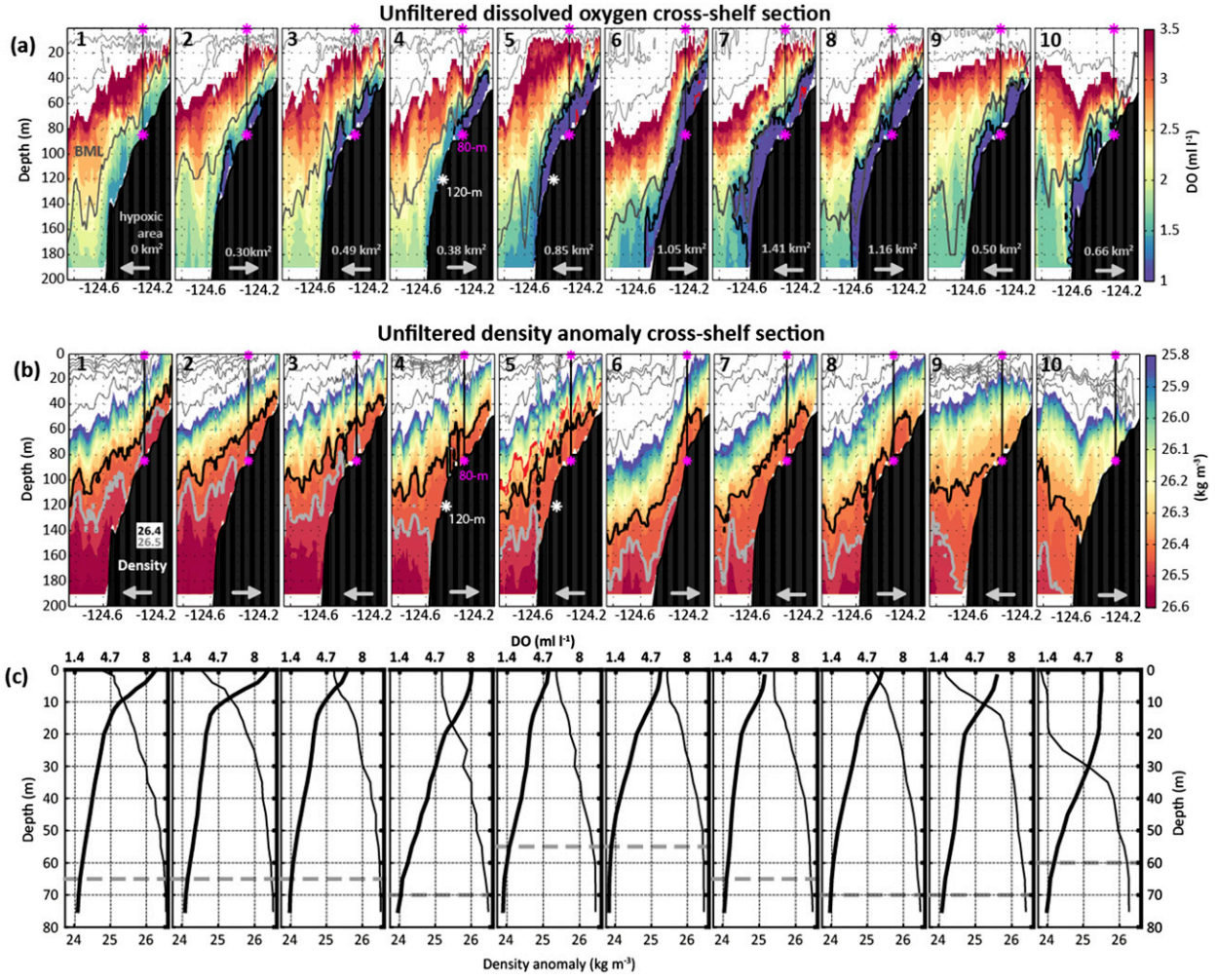

FIG. 4. (a) DO and (b) density data for Slocum glider cross-shelf section sequence (1–10) along the NH-Line, 8 Aug–27 Sep 2011. In (a), DO (ml L^{-1}) data are color contoured for the concentration range 0–3.5 ml L^{-1}. The hypoxic contour (1.4 ml L^{-1}) is shown in black and the BML in dark gray. Shallow-oxygen contours (5 and 7 ml L^{-1}) are plotted as light gray contours. The 80-m (120 m) isobath crossing is noted by pink (white) stars. The hypoxic cross-sectional area of each line is maximum (1.41 km^2) in line 7. In (b), potential density anomaly (kg m^{-3}) data are color contoured (25.8–26.6) and line contoured 23–25.8. Isopycnals 26.4 (black) and 26.5 (gray) are near bottom. Cross-shelf sections in (a) and (b) are organized offshore to onshore with an arrow indicating direction of glider path. Time increases left to right for even glider lines. (c) Vertical profiles of DO (thick) and density at the 80-m isobath crossing are plotted for each glider line in (a) and (b), with the BML height (dashed).

midshelf DO levels have increased significantly, and hypoxia is only observed on the outer shelf.

The 26.5 kg m^{-3} isopycnal is observed on the shelf in line 1 and off the shelf in lines 2–10 with increasing depth. This behavior is also observed in shallower isopycnals. The onshore upward tilt of interior isopycnals and oxygen contours is observed in lines 1–8. In line 9, the 3.5 ml L^{-1} and 25.8 kg m^{-3} isopleths are flat. By line 10, a downward tilt is observed, indicative of the fall transition to downwelling-favorable conditions. This is expected since line 10 was sampled directly after a strong poleward wind event (Figs. 2a, 3a), characteristic of the fall transition to downwelling-favorable conditions. The vertical profile of density during line 10 (Fig. 4c) shows a well-mixed top and bottom 20 m, indicating strong and deep mixing in both boundary layers.

As shown in Fig. 4c, near-bottom density decreases throughout the glider line sequence on the 80-m isobath. In 2011, offshore source waters (NH25; Fig. 1) at densities upwelling onto the shelf were found to have a strong relationship of a 0.32 ml L^{-1} increase in DO per 0.1 kg m^{-3} density decrease (Adams et al. 2013). However, the decrease in near-bottom density observed in the 10 glider lines is not associated with an increase in near-bottom DO (Figs. 4a,b). This is because of the strong influence of shelf processes and

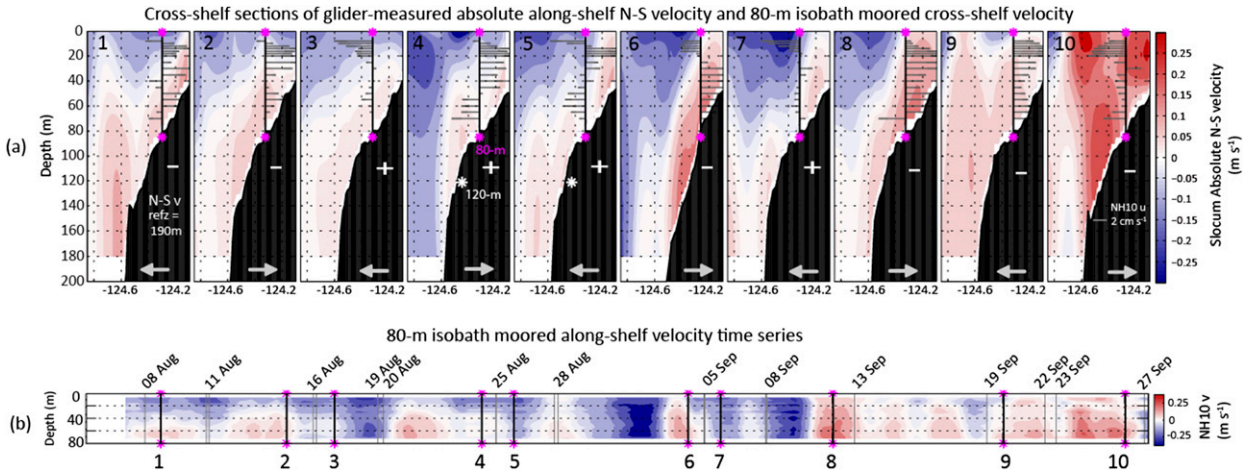

FIG. 5. (a) Glider line sequence of absolute N–S velocity (geostrophic- + glider-measured depth averaged). The geostrophic velocity (not shown) reference depth is 190 m. Positive velocities are poleward. Depth profiles of NH10 cross-shelf velocity horizontal bars (gray) plotted over the 80-m isobath correspond to the time of the glider's 80-m isobath crossing (pink stars). Offshore (negative) E–W velocities are pointing left. For scale, a 2 cm s^{-1} vector is shown in line 10. The sign of cross-shelf bottom Ekman layer flow, values in Table 1, is shown in each panel as a + or − for onshore or offshore flow, respectively. (b) Midshelf mooring (NH10; 80-m water depth) ADCP along-shelf velocity (m s^{-1}) low-pass filtered (40-h) time series for 7–73-m depth range. Gray lines indicate start and stop times of each glider line (1–10), whereas black lines and stars indicate glider 80-m isobath crossings.

local respiration on intraseasonal near-bottom DO variability.

As presented in section 3a, time-integrated currents (Fig. 3b) indicate that the onshore return flow during late summer 2011 occurs at ~30-m water depth over the 80-m isobath, not in the BBL. From the vertical profiles of density over the 80-m isobath (Fig. 4c), stratification is constant at 30 m, which indicates that this is an interior depth, outside of the surface and bottom mixed layers, except in section 10. Note that DO at 30 m, the return flow depth, is above the hypoxic threshold in each glider line (Fig. 4a).

3) Absolute velocity

Lines of glider-derived absolute N–S velocity v_{abs} are presented in Fig. 5a. The strong equatorward (blue) surface flow observed offshore of the 80-m isobath in Fig. 5a is the coastal upwelling jet, which varies in strength and location throughout the 10 lines. Throughout the upwelling season, the coastal jet moves offshore and widens in cross-shelf extent following the 100–200-m isobaths around the Heceta and Stonewall Bank complex (HSBC; Barth et al. 2005). Near-bottom poleward flow is observed on the shelf, although varying in strength and location in between glider sections. This supports the previous moored current result of late upwelling season reversals in the near-bottom current direction unlike earlier in the season when near-bottom along-shelf currents are strongly equatorward (Fig. 2e).

The N–S moored velocity v_{NH10} time series from the 80-m isobath is plotted in Fig. 5b to show the variability and structure of along-shelf currents throughout the glider line sequence. Each glider crossing of the 80-m isobath is marked by a black line. These data are also used in the v_{abs} and v_{NH10} mooring data comparison in Figs. A1–A2. Poleward near-bottom flows observed in Fig. 5a are also observed in the v_{NH10} record in Fig. 5b.

4) Measured cross-shelf velocities and bottom Ekman transport

Low-pass filtered moored cross-shelf current data u_{NH10} is included as horizontal bars in Fig. 5a over the 80-m isobath. Onshore flow is nonzero at interior depths (40–60 m) for all lines. Moored current records presented in section 3a show a main return flow depth at 30 m when near-bottom flow becomes weak (Fig. 3c). The seasonal decline in BBL cross-shelf transport U_b^{Ek} shown in Fig. 3d suggests that the BBL during the glider line sequence is arrested (Garret et al. 1993). Diminished flow in the BBL implies decreased near-bottom flushing rates. The term U_b^{Ek} is calculated for each glider line from the moored current record, following the formulation presented in section 3a. The sign of U_b^{Ek} is indicated as a + or − sign in each panel of Fig. 5a. The observed near-bottom cross-shelf flow at 60 m is the same direction as U_b^{Ek} except in glider line 10. The agreement is not as strong at 70 m for lines 1, 7, 8, and 10.

c. *Physical versus biological drivers of intraseasonal DO variability*

Variability of near-bottom DO shown in Figs. 2c and 4a is quantified and investigated using the 10 glider lines presented in section 3b. Specifically, we focus on the difference between consecutive glider sections of DO and density 10 mab at the midshelf (80-m isobath; 0.2% slope; 18 km offshore) and the outer shelf (120 m; 0.7%; 30 km offshore). The horizontal separation of these stations is 12 km. Potential mechanisms responsible for changes in observed DO between glider lines that can be estimated with extant data include local water column respiration, cross-shelf advection, and along-shelf advection. Other mechanisms that cannot be estimated here, such as vertical and horizontal mixing and benthic respiration, are addressed in the discussion.

1) TREND OVER GLIDER SEQUENCE

Near-bottom DO data extracted from the unfiltered gridded glider sections shown in Fig. 4a are lower at the outer shelf (120 m) than over the midshelf (80 m) for the majority of the glider line sequence (Figs. 6a,c). Lower DO water on the outer shelf is counter to the idea of higher DO source water flowing onshore, replenishing near-bottom waters (Adams et al. 2013). Two hypotheses for why outer shelf DO concentrations are lower than over the midshelf include 1) cross-shelf flow is offshore and near-bottom DO concentrations are declining on route to the outer shelf from local microbial respiration and 2) a low DO along-shelf gradient is transported either north or south to the NH-Line. We evaluate these hypotheses using moored midshelf currents at NH10 and the glider data.

Time-integrated cross-shelf and along-shelf currents, or CD, calculated from the NH10 ADCP record, are quantified for the glider lines in Table 3. Weak offshore transport of low DO midshelf water occurred during the majority of the glider sequence, as first shown in Fig. 3c. However, the magnitude of cross-shelf CD, up to 8 km in the offshore direction, is smaller than the 12-km horizontal separation between the mid- and outer shelf stations. Therefore, offshore cross-shelf advection cannot explain the abrupt downslope extension of the hypoxic shelf area observed in lines 5–8 (Fig. 4a).

Along-shelf CD values are variable in direction and magnitude throughout the glider line sequence. During glider lines 2–8, along-shelf CD is small and/or negative. This indicates equatorward flow, observed between 80-m crossings in Fig. 5b. During glider lines 2–8 is when the downslope extension of the hypoxic area occurs. If along-shelf advection of a low DO gradient caused this change, it would be from about 2 to 40 km north of the NH-Line. In line 6, observations of low DO water across the shelf were collected as the glider detoured far off course to the north of the NH-Line (Fig. 1). Advection of this low DO water southward to

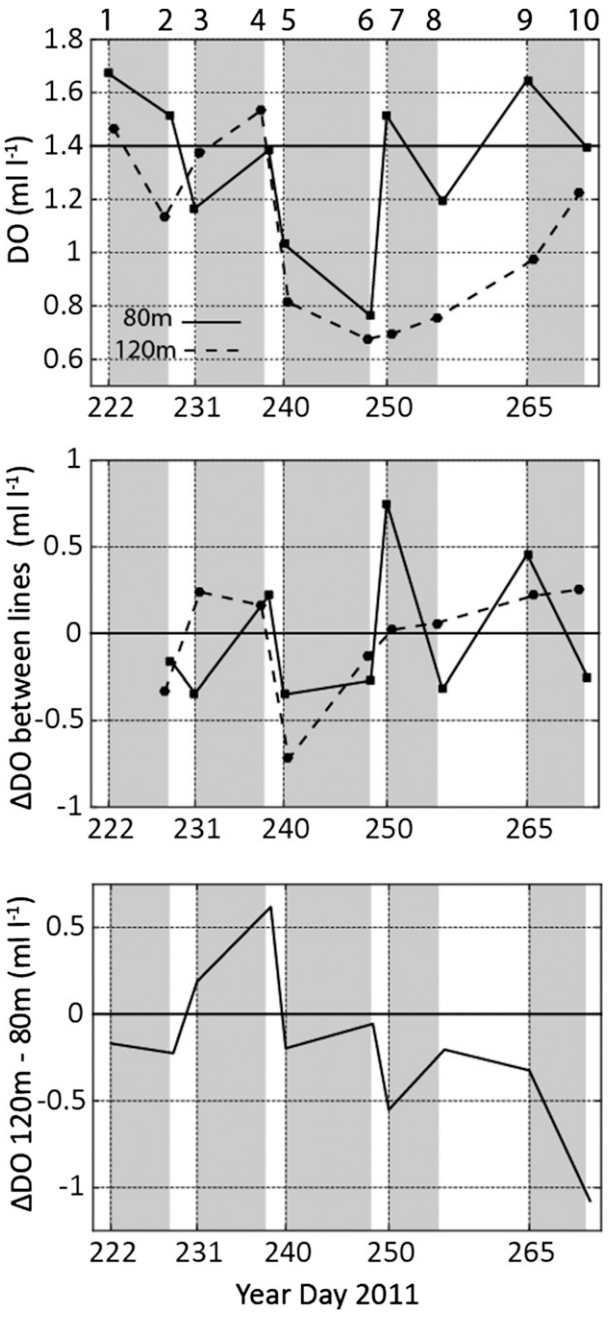

FIG. 6. (a) Dissolved oxygen (ml L^{-1}) measured 10 m above the bottom at the 80- (solid) and 120-m (dashed) isobath crossings of each glider line 1–10 (Fig. 1). (b) Change in near-bottom DO values 10 m above the 80- and 120-m isobaths between consecutive glider lines. (c) Difference of outer-shelf and midshelf DO values, 120–80 m, for each glider line.

TABLE 3. Time integration of NH10 (44.65°N, −124.3°W, 80-m water depth) N–S and E–W measured near-bottom average (69–73 m) water velocities between sequential glider section 80-m isobath crossings yields cumulative displacements (km). Positive values are poleward (north) and onshore (east). Time integration starts at 80-m isobath crossing of one line and stops at 80-m isobath crossing of next line (i.e., section 1 to 2).

Glider lines	ADCP time integration start time (yearday 2011 UTC)	N–S 80-m cumulative displacement (km)	E–W 80-m cumulative displacement (km)
2–1	221.81	17.72	−5.73
3–2	228.20	−4.81	−1.57
4–3	230.63	−4.38	−6.76
5–4	238.13	−2.58	−1.39
6–5	239.75	−32.12	−3.80
7–6	248.62	0.10	−0.62
8–7	250.27	−23.21	−0.02
9–8	255.98	37.70	2.36
0–9	264.65	56.63	−8.76

the NH-Line could explain the downslope extension of near-bottom hypoxia.

2) CHANGE IN OUTER SHELF DO BETWEEN CONSECUTIVE GLIDER LINES

Observed DO rates of change are calculated in between consecutive glider lines in Table 2. Using the density DO relationship of source water (NH25; Fig. 1) presented in Adams et al. (2013), an expected DO rate of change based on the observed density change between lines is calculated as $0.32\,\mathrm{ml\,L^{-1}}$ $(0.1\,\mathrm{kg\,m^{-3}})^{-1}$. Similarly, the expected drawdown of DO from respiration is estimated from an average respiration rate calculated at SH70 ($0.026 \pm 0.013\,\mathrm{ml\,L^{-1}\,day^{-1}}$; Adams et al. 2013). The observed DO rates of change range from −0.13 to 0.29 and from −0.45 to $0.10\,\mathrm{ml\,L^{-1}\,day^{-1}}$ on the mid- and outer shelf regions, respectively. The magnitude of this event-scale variability is similar for DO decreases and increases of the mid- and outer shelf. Moreover, this variability on short time scales is many times larger than the observed seasonal DO decline observed on the central Oregon shelf ($\sim 0.01\,\mathrm{ml\,L^{-1}\,day^{-1}}$; Adams et al. 2013).

The largest change in outer-shelf DO between any two consecutive glider lines is observed between lines 4 and 5 (Figs. 6a,b). At 120 m, DO decreased by $0.72\,\mathrm{ml\,L^{-1}}$ in 2.8 days, whereas the 80-m DO values dropped by half that amount, $0.35\,\mathrm{ml\,L^{-1}}$, in 1.5 days (Fig. 6b; Table 2). The respective DO decline rates of these sharp decreases are 0.45 and $0.13\,\mathrm{ml\,L^{-1}\,day^{-1}}$, respectively, which are several times larger than the average local respiration rate. This rules out local respiration as the driving mechanism of the observed DO decrease between glider lines 4 and 5 at the mid- and outer-shelf stations and also the sharp increase in hypoxic area downslope (Fig. 4a).

Cross-shelf CD between the 80-m isobath crossings of glider sections 4 and 5 is −1.39 km (Table 4). This indicates that a water parcel starting at the 80-m isobath does not travel far offshore between lines 4 and 5; cross-shelf advection therefore cannot explain the observed downslope extension of hypoxic area in line 5 (Fig. 4a). Furthermore, DO concentrations onshore of 120 m are higher during this time (Figs. 6a,b), so cross-shelf advection of a gradient cannot be the driving mechanism of the extension of the hypoxic area down the slope.

Since the N–S CD is negative, along-shelf advection of a low DO gradient from the north is likely. Low DO shelf water north of the line is observed in glider line 6, which sampled up to 14 km north of the NH-Line. Along-shelf advection of a gradient is the most plausible driving mechanism of the observed DO decline between glider lines 4 and 5. The magnitude of this gradient is the observed DO decline at 120 m divided by the along-shelf CD ($0.72\,\mathrm{ml\,L^{-1}}/2.58\,\mathrm{km}$ or $0.28\,\mathrm{ml\,L^{-1}\,km^{-1}}$). Similarly, the magnitude of the along-shelf DO gradient is only $0.14\,\mathrm{ml\,L^{-1}\,km^{-1}}$ over the 80-m isobath. Here, we have assumed the midshelf CD applies to the outer shelf. There is evidence from the Coastal Advances in Shelf Transport (COAST) 2001 (Boyd et al. 2002) program that near-bottom currents are correlated strongly across the shelf with a 0.65 cross-correlation coefficient at zero lag.

Along-shelf maps of low DO waters in the upper 200 m along the northern CCS indicate strong along-shelf gradients north of the NH-Line in September 2011 with a minimum north of the NH-Line over the shelf break (Peterson et al. 2013). This supports our hypothesis that equatorward along-shelf advection of a low DO water is the mechanism responsible for the large decline in DO observed between glider sections 4 and 5.

TABLE 4. Mean and standard deviation of glider-measured hypoxic water mass properties sampled along the NH-Line (44.67° to 44.7°N) from 2006 to 2012, as shown in Fig. 8.

Isobath (m)	Latitude (°N)	Longitude (°W)	Temperature (°C)	Salinity	σ_θ (kg m^{-3})	Pressure (m)	DO (ml L^{-1})
50	44.67 ± 0.01	124.14 ± 0.01	7.62 ± 0.2	33.85 ± 0.06	26.43 ± 0.07	40 ± 8	1.08 ± 0.2
80	44.67 ± 0.01	124.29 ± 0.01	7.51 ± 0.3	33.88 ± 0.05	26.46 ± 0.07	67 ± 9	1.00 ± 0.3
100	44.67 ± 0.01	124.41 ± 0.01	7.64 ± 0.2	33.86 ± 0.05	26.43 ± 0.06	86 ± 11	1.13 ± 0.2
120	44.67 ± 0.02	124.48 ± 0.02	7.58 ± 0.3	33.88 ± 0.04	26.45 ± 0.06	104 ± 11	1.12 ± 0.2
200	44.66 ± 0.02	124.58 ± 0.02	7.47 ± 0.3	33.93 ± 0.04	26.51 ± 0.07	147 ± 25	1.17 ± 0.2
250	44.67 ± 0.01	124.63 ± 0.01	7.29 ± 0.3	33.94 ± 0.05	26.54 ± 0.08	157 ± 24	1.25 ± 0.1

d. Cross-shelf variability of hypoxic observations (2006–12)

1) LOCATION OF HYPOXIC MEASUREMENTS

The glider lines previously presented from 2011 are 10 out of 249 cross-shelf NH-Line sections taken from April 2006 to December 2012. Hypoxia is observed in 133 glider lines total. The glider paths of those 133 lines are plotted in Fig. 7a with the hypoxic section highlighted in blue. The large, along-shelf spread of glider lines is due to the slow vehicle speed of the Slocum gliders compared to the coastal currents. Hypoxia is observed each year in the dataset and across the

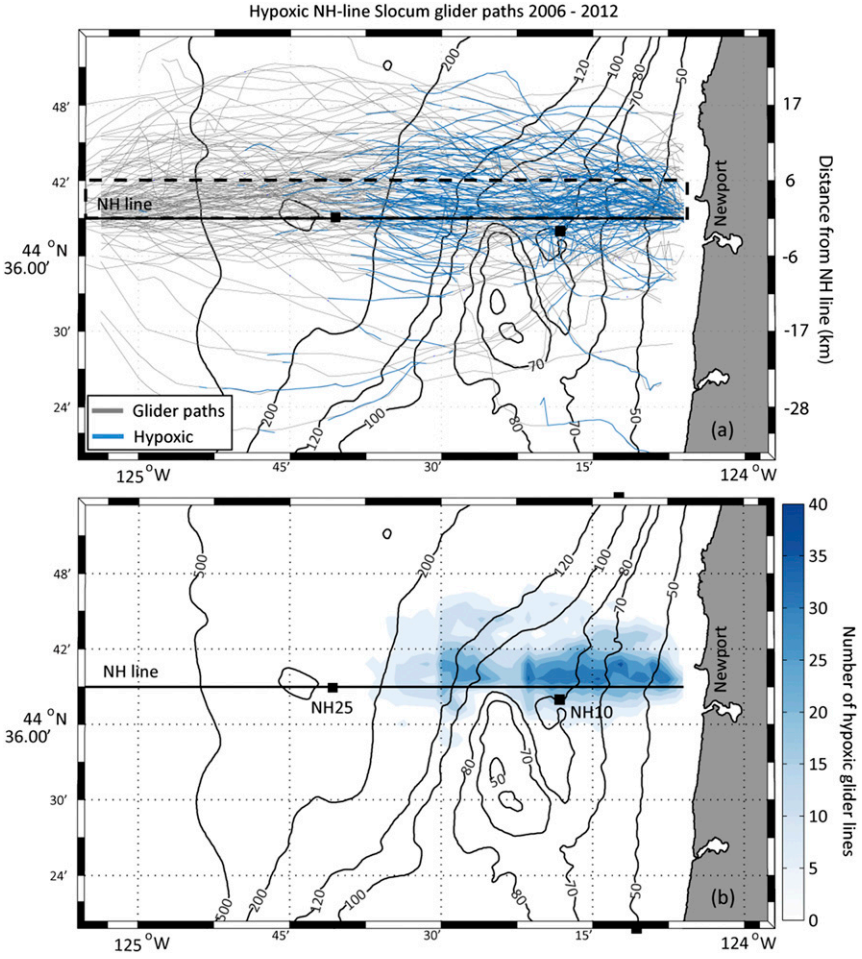

FIG. 7. (a) Map of 133 Slocum glider paths in which hypoxia was measured along the NH-Line from 2006 to 2012 in gray. Blue lines correspond to the section of each glider line where hypoxia was observed. Observations outside of the dashed box are not considered to be along the NH-Line. (b) Colored histogram map of hypoxic glider line measurements of glider paths in (a) showing two separate prevalent hypoxic areas.

continental margin. A colored histogram map of hypoxic glider line sections in Fig. 7a reveals areas across the shelf where hypoxia is recurrent (Fig. 7b). The midshelf, between the 50- and 80-m isobaths, is the region across the NH-Line with the most hypoxic measurements, although hypoxia is also often observed in a second region on the outer shelf (120 to 200 m).

The vertical cross-section histogram of the 98 hypoxic glider lines across the NH-Line, 44.64°–44.70°N, is shown in Fig. 8a. Two distinct cross-shelf regions with prevalent hypoxic measurements are the mid- (50–80-m isobaths) and outer shelf (120–200-m isobaths), similar to glider lines 2, 3, and 9 in Fig. 4a. Hypoxia is observed over the midshelf in over 40% of the hypoxic glider lines, whereas outer-shelf hypoxia is observed in only 30% of hypoxic glider lines. Results presented in section 3c indicated lower DO over the outer shelf. This is most likely a late-season result after onshore cross-shelf flow shuts down and near-bottom outer-shelf waters are no longer replenished with source water. Mean dissolved oxygen and density values are presented for the cumulative hypoxic glider lines in Fig. 9a. Between the two locations of prevalent hypoxia, dissolved oxygen is higher and density is lower than the surrounding shelf values (Figs. 8b,c). A mechanism for this is discussed in section 4.

Given that most of the glider transects are close to the NH-Line (Fig. 7), it is difficult to determine the along-shelf extent of the two distinct cross-shelf regions with prevalent hypoxia. Fortuitously, glider line 6 (Fig. 1) was sampled ~5–10 km north of the NH-Line and showed contiguous near-bottom hypoxia across the shelf (Fig. 4b).

Hypoxia is observed offshore around station NH25 in less than 2% of the NH-Line hypoxic glider lines. This station is often used as an upwelling source water location (Adams et al. 2013; Peterson et al. 2013). Infrequent hypoxia at NH25 is from near-bottom hypoxic shelf waters extending offshore as shown in glider line 7 (Fig. 4a). Since the top of the North Pacific oxygen minimum zone (OMZ) is at approximately 400-m water depth (Pierce et al. 2012), hypoxic measurements made in the top 200 m are attributed to shelf-influenced low DO waters rather than the upwelling of OMZ water.

2) Water mass properties of hypoxic measurements

Variability of water mass properties (DO, temperature, salinity, density, and pressure) is presented at several isobath crossings along the NH-Line for all glider-measured hypoxic measurements (Table 4). Oxygen values of hypoxic measurements are more concentrated near the hypoxic threshold at 250-m isobath

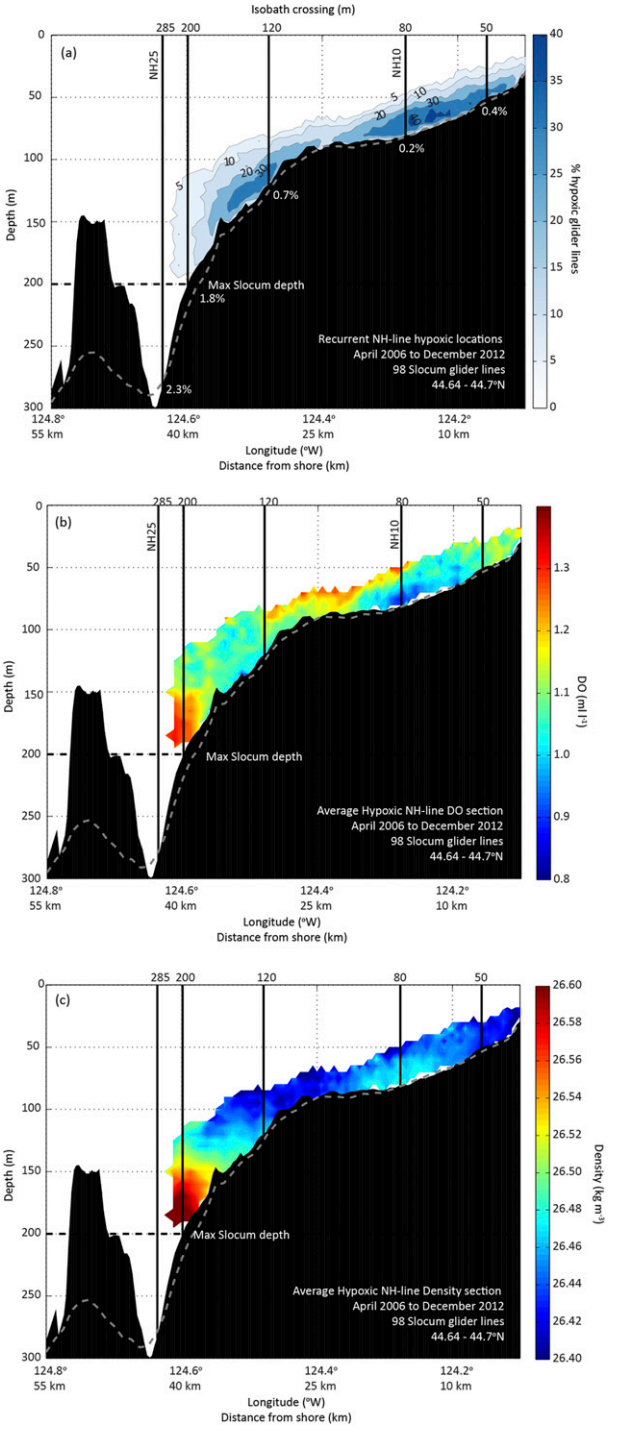

FIG. 8. (a) Sum of glider-measured hypoxic occurrences (blue) from filtered, gridded Slocum glider cross-shelf sections (2006–12) along (a) the NH-Line (44.64° to 44.7°N) for the top 200 m of the water column. The average glider-line bottom depth (dashed) is smoother and more monotonic than actual bathymetry (black). Bottom slope (%) for the 50-, 80-, 120-, 200-, and 285-m isobath crossings along the NH-Line are based on the actual bathymetry (black). Average (b) DO and (c) density sections corresponding to the hypoxic glider lines shown in (a).

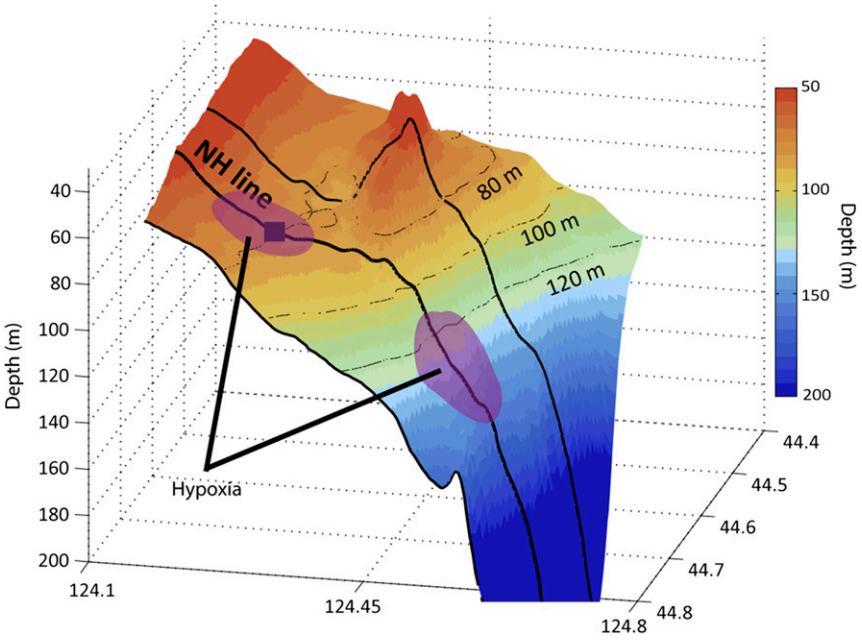

FIG. 9. Central Oregon continental shelf bathymetry with latitudinal contours at 44.55°, 44.65° (NH-Line), and 44.75°N. The 80-, 100- and 120-m isobaths are also included in black. Hypoxic zones often observed on the NH-Line are on either side of the sharp topographic feature to the south, Stonewall Bank.

versus the 70-m isobath where there is a larger spread of DO values. This further supports the previous result of prevalent hypoxia over the midshelf throughout the 2006 to 2012 upwelling seasons.

Temperature, salinity, and density all have more normal distributions with peaks warming, freshening, and lightening onshore, respectively. Pressure indicates the depth over each isobath crossing where hypoxic measurements are recorded. Over the 50- and 70-m isobaths, the majority of the measurements are made ~10 mab. The 100-m isobath distribution indicates that hypoxic measurements are also likely 20 mab. This could be due to higher average BML (Table 1). Over the 200-m isobath, the pressure distribution of hypoxic measurements is very spread out from 100- to 190-m depths.

4. Discussion

a. *Cross-shelf DO variability caused by along-shelf advection*

To the south of the NH-Line is the HSBC, a very productive, retentive area (Barth et al. 2005) where persistent hypoxia ~3 months a year is observed on the midshelf (Adams et al. 2013). When flow is poleward, hypoxic waters from the bank would be advected to the NH-Line. In fact, after a 20-km poleward CD (Table 3) between glider lines 1 and 2, near-bottom hypoxic water was observed over the mid- and outer-shelf regions (Fig. 4a). Along-shelf advection of low DO patches $O(10)$ km has been identified as a driver of low DO variability on the Washington shelf (Connolly et al. 2010).

Here, two distinct regions of prevalent hypoxia are identified (Figs. 7b, 8a). The cross-shelf gap, $O(10)$ km, between the two NH-Line prevalent hypoxic regions is directly to the north of Stonewall Bank, shown on a bathymetric map of the region in Fig. 9. Observations of BBL mixing over Stonewall Bank are several orders of magnitude larger than the background shelf-mixing rate under upwelling-favorable conditions early in the upwelling season (Nash and Moum 2001). We hypothesize that strong mixing during poleward flow around this feature also increases mixing rates in the BBL over the bank. Increased mixing would be a source of DO for the BBL due to entrainment of shallower, interior waters. The high DO signal observed in between the two cross-shelf hypoxic areas in Figs. 7b and 8a are likely due to mixing over Stonewall Bank that is advected northward to the NH-Line. The gap between the two prevalent hypoxic areas on the NH-Line corresponds to a region of increased DO and decreased density (Figs. 8b,c) in average vertical cross-shelf sections corresponding to the

hypoxic glider lines (Fig. 8a). This suggests that less dense, higher DO water is vertically mixed into the BBL over Stonewall Bank and advected northward to the NH-Line. To test this theory of whether high DO water is prevalent northward of Stonewall Bank during northward flow, glider-derived N–S velocities are used to investigate the relationship between flow direction and the difference in DO 10 mab over the 100- and 80-m isobaths during hypoxic events. Here, we expect a positive near-bottom DO difference, 100–80 m, during times of positive flow direction. For all but one of the instances when hypoxia is observed over the 80-m isobath (squares in Fig. 10) and when N–S velocities and DO differences are large (outside the gray bar regions in Fig. 10), strong poleward flow is associated with DO values that are significantly higher over the 100-m isobath than over the 80-m isobath in the lee of Stonewall Bank.

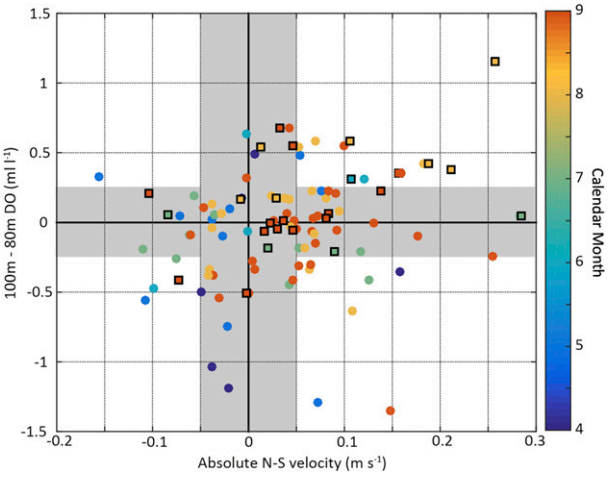

FIG. 10. Glider-derived, near-bottom N–S velocities v_{abs} from 10 mab the 100-m isobath plotted against the cross-shelf difference in near-bottom DO, 100–80 m, for Slocum glider lines sampled between 44.64° to 44.7°N. Colors indicate month of year, April–September. Regions of the plot with low DO concentrations or poleward velocities are shaded.

b. Return flow depth

1) IMPLICATIONS FOR HYPOXIA

Moored time series of midshelf water velocities from the 2011 upwelling season show the onshore return flow depth changes from near bottom (70 m) around day 190 to an interior depth of 30-m water depth (Fig. 3b). After the shoaling of the return flow depth, 1) the near-bottom flow stalls in both along- and cross-shelf directions increasing retention of near-bottom waters and 2) a shutdown of source water upwelling on to the shelf results in a near-bottom temperature increase (McCabe et al. 2015) and density decrease (Fig. 2b) contrasting to the cool, salty signature of source water present early in the upwelling season. A combined decrease of flushing and source water replenishment of near-bottom shelf waters increases the risk for late-season near-bottom hypoxia. This is supported by the moored 2011 DO time series (Fig. 2c), which does not show persistent hypoxia until after day 190, when the BBL flow weakens.

2) MECHANISMS

In a two-dimensional upwelling model over a slope bottom, Lentz and Chapman (2004) find nonlinear cross-shelf momentum flux divergence to cause return flow below the surface boundary layer when the slope Burger number S is 1.5–2. High values of $S = N\alpha f^{-1}$, where N is the buoyancy frequency, α is the cross-shelf bottom slope, and f is the Coriolis parameter, were found for Oregon coast data from 45°N where the shelf slope is steep and

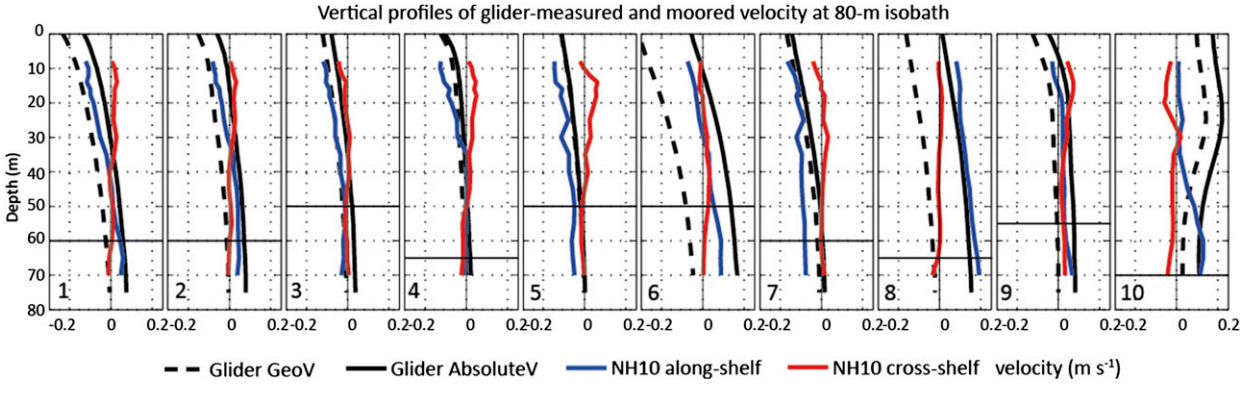

FIG. A1. Vertical profiles of glider geostrophic velocity (black dashed) referenced to 190 m, glider absolute velocity (black), and moored NH10 along-shelf (blue) and cross-shelf (red) velocities all over the 80-m isobath. The moored NH10 profiles were extracted from the continuous time series at the time of each glider line 80-m isobath crossing (Table 1).

the bathymetry variations are small. Interior return flow is observed in a single cross-shelf velocity depth profile (Smith 1981). To be consistent with the Lentz and Chapman (2004) prediction, S should be low early in the season when we observe BBL return flow and high late in the season when return flow is observed ~30 m. However, we find that stratification, and, therefore S, decreases throughout each upwelling season.

Another proposed mechanism for the late-season onshore interior flow is the presence of an along-shelf pressure gradient. McCabe et al. (2015) report a decrease in sea level along the U.S. West Coast from July to September, resulting in a mean poleward pressure gradient along the CCS late in the upwelling season. The authors attribute the late-season onshore interior flow to this poleward pressure gradient suggesting that the shoaling of return flow depth is driven remotely rather than locally, for example, pressure gradient over Heceta Bank. Further investigation is needed to sufficiently correlate the development of the large-scale poleward pressure gradient and the observed intraseasonal decrease of near-bottom onshore transport at NH10.

Previous studies have identified the complicated three-dimensional flow regime over the central Oregon shelf. Smith (1981) found an imbalance between the onshore transport below the surface and the offshore surface transport from moored current data on the Oregon shelf and concludes the dv/dy continuity term cannot be neglected. Barth et al. (2005) and Hales et al. (2006) attribute an unsteady wind field and variations in the bathymetric features to the three-dimensional flow fields in this region. Coastal circulation along the NH-Line is likely three-dimensional because of the combination of temporal variations in wind forcing and spatial variations in bathymetric features.

c. *Future observational needs*

With the addition of underwater gliders as observational platforms, finescale, cross-shelf resolution of measurements has increased; however, along-shelf resolution is still lacking. We have identified the lack of high-resolution (<10 km), along-shelf DO data and of cross-shelf current data over the central Oregon shelf. To date, no study has captured the along-shelf component to near-bottom DO variability on seasonal time scales. Additionally, future experiments should include observations of the BBL if possible. As part of the NSF-funded Ocean Observatories Initiative (OOI) Endurance array, gliders will occupy one along-shelf and multiple cross-shelf transects over the Oregon and Washington continental shelf. These data should enable the finescale resolution across and along the continental shelf not currently possible.

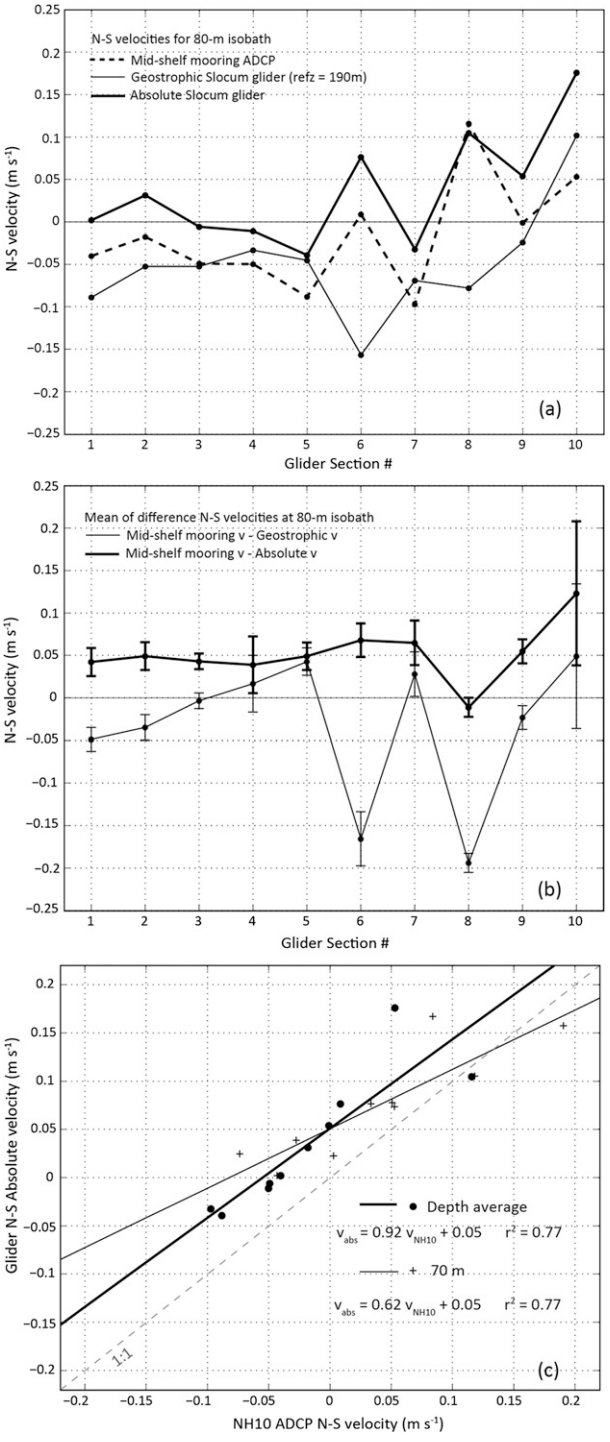

FIG. A2. (a) Depth-averaged N–S velocities at the NH-Line 80-m isobath from the midshelf NH10 mooring (dashed), Slocum glider geostrophy (black), and Slocum glider absolute (bold) for the NH-Line glider sections (1–10) in Fig. 1. (b) Mean and standard deviation of the difference between the mooring and glider N–S velocity vertical profiles at each 80-m isobath crossing. (c) NH10 mooring ADCP N–S velocities vs Slocum glider absolute N–S velocities, depth averaged (circles) and 70 m (crosses). Linear regression lines and skills, r^2 values, are shown for depth-averaged (bold) and 70-m (black) N–S velocity data.

TABLE A1. Difference between the depth average and 70-m water depth NH10 moored ADCP and glider-derived N–S velocities during the 10 glider lines shown in Fig. 1.

Glider line no.	Depth average		70-m depth	
	$v_{abs} - v_{NH10}$	$v_{geo} - v_{NH10}$	$v_{abs} - v_{NH10}$	$v_{geo} - v_{NH10}$
1	0.042 ± 0.016	−0.049 ± 0.014	0.021	−0.064
2	0.049 ± 0.016	−0.035 ± 0.015	0.043	−0.038
3	0.043 ± 0.009	−0.003 ± 0.009	0.066	0.020
4	0.039 ± 0.033	0.017 ± 0.033	0.020	−0.003
5	0.049 ± 0.016	0.043 ± 0.016	0.045	0.039
6	0.068 ± 0.020	−0.166 ± 0.032	0.083	−0.131
7	0.065 ± 0.026	0.028 ± 0.026	0.098	0.062
8	−0.011 ± 0.011	−0.194 ± 0.011	−0.033	−0.216
9	0.055 ± 0.014	−0.023 ± 0.014	0.027	−0.051
10	0.123 ± 0.085	0.049 ± 0.085	−0.013	−0.087

5. Summary and conclusions

Cross-shelf variability of near-bottom dissolved oxygen concentrations on intraseasonal and interannual time scales is resolved (<1 km) using Slocum glider lines along the Newport hydrographic line. A sequence of 10 glider cross-shelf sections spanning 50 days clearly shows large intraseasonal variability on day–month time scales. Late-season return flow depth is observed at 30 m, while near-bottom cross-shelf flow is weakly offshore. The change in return flow depth is not associated with a change in stratification. Outer-shelf DO decreases during the sequence but cannot be linked with the cross-shelf advection of a gradient or drawdown due to local respiration. Therefore, an along-shelf gradient is found to be responsible for the largest DO decline observed in the glider line sequence. Hypoxia is prevalent on the mid- and outer-shelf regions in two distinct regions. Enhanced mixing over the sharp topographic feature of Stonewall Bank to the south of the NH-Line is a likely cause of the separation of the two cross-shelf hypoxic zones.

Acknowledgments. Foremost, we thank our OSU glider group colleagues, A. Erofeev, Z. Kurokawa, P. Mazzini, C. Ordonez, A. Sanchez, G. Salidias, T. Peery, J. Brodersen, and L. Rubiano-Gomez, for their combined 6+ yr of glider data collection efforts along the Newport hydrographic line supported by National Science Foundation (NSF) Grants OCE-0527168 and OCE-0961999. A. Erofeev is additionally thanked for assistance with glider pilot training, optode calibration, and glider data processing. Thanks to J. Jennings and A. Ross for their assistance with Winkler titrations for optode calibrations. In kind memory, M. Levine provided invaluable guidance and the NH10 mooring data. SH70 mooring data were collected through the MI_LOCO program funded by Gordon and Betty Moore Foundation (Grant 1661). Thanks to Francis Chan for SH70 thoughtful comments. Special thanks to W. Waldorf, C. Risien, and D. Langner for NH10 data processing and assistance in the field. We also thank Captain Mike Kriz, the crew of the R/V *Elakha*, and the OSU Marine Technician Group for their data collection efforts.

APPENDIX

Comparison of Midshelf Moored versus Glider-Derived N–S Velocities

Vertical profiles of v_{NH10}, u_{NH10}, v_{abs}, and v_{geo} over the 80-m isobath are compared in Fig. A1. Negative vertical shear, or increasing N–S velocity with depth, is observed in each moored vertical profile consistent with thermal wind and $\partial\rho/\partial x$ (Fig. 4c). The same is true for the glider velocity profiles except for section 10 (Fig. 5a).

Depth-averaged N–S velocities from the two different platforms, the NH10 mooring and the glider, are compared in Fig. A2. Moored ADCP data are selected at the time of each glider 80-m isobath crossing (Table 1) and interpolated onto the glider depth grid (2–5-m vertical spacing). Depth-averaged velocities are calculated for the water depth range of 8–70 m since the top 7 m are not measured by the downward-looking ADCP.

The depth-averaged v_{geo} and v_{abs} over the 80-m isobath are plotted alongside the depth-averaged v_{NH10} at the time of each glider 80-m isobath crossing. Overall, v_{NH10} and v_{abs} compare qualitatively well; however, v_{abs} has a weaker magnitude in most glider sections. This signal dampening is a result of filtering the glider data or the measurement of v_{abs} over several vertical glider profiles. The average of the difference between the glider-measured and moored N–S velocities at each depth in the vertical profiles (Fig. A1) are presented in

Fig. A2b and Table A1. The depth-averaged v_{abs} is approximately 0.05 m s^{-1} more poleward than v_{NH10} in each glider lines except for 8 and 10. However, v_{geo} differences vary erratically and as large as 0.2 m s^{-1} more equatorward than v_{NH10}.

Depth-averaged and near-bottom (70 m) v_{NH10} and v_{abs} are compared further in Fig. A2c. The depth-averaged linear regression line slope (0.92) is much closer to 1 than the 70-m slope of 0.62; however, an offset of 0.05 m s^{-1} is found for both datasets. The rms deviations for the depth-averaged and 70-m regression analysis are 0.031 and 0.026 m s^{-1}, respectively. Previously reported linear regressions (offset -0.02 m s^{-1}) with similar r^2 values compared measured water velocities and calculated geostrophic velocities referenced to 500 dbar from NH10 at 30-m water depth (Huyer et al. 2005). The v_{abs} offset could be attributed to the shallow reference depth of the geostrophic calculation, 190 m, or to compass inaccuracy.

REFERENCES

Adams, K. A., J. A. Barth, and F. Chan, 2013: Temporal variability of near-bottom dissolved oxygen during upwelling off central Oregon. *J. Geophys. Res. Oceans*, **118**, 4839–4854, doi:10.1002/jgrc.20361.

Barnes, S. L., 1964: A technique for maximizing details in numerical weather map analysis. *J. Appl. Meteor.*, **3**, 396–409, doi:10.1175/1520-0450(1964)003<0396:ATFMDI>2.0.CO;2.

Barth, J. A., S. D. Pierce, and R. M. Castelao, 2005: Time dependent, wind-driven flow over a shallow mid shelf submarine bank. *J. Geophys. Res.*, **110**, C10S05, doi:10.1029/2004JC002761.

Boyd, T., M. D. Levine, P. M. Kosro, S. R. Gard, and W. Waldorf, 2002: Observations from Moorings on the Oregon Continental Shelf, May-August 2001: A component of Coastal Advances in Shelf Transport (COAST). COAS Data Rep. 190, Reference 2002-6, 124 pp.

Castelao, R. M., and J. A. Barth, 2005: Coastal ocean response to summer upwelling favorable winds in a region of alongshore bottom topography variations off Oregon. *J. Geophys. Res.*, **110**, C10S04, doi:10.1029/2004JC002409.

Chan, F., J. A. Barth, J. Lubchenco, A. Kirincich, H. Weeks, W. T. Peterson, and B. A. Menge, 2008: Emergence of anoxia in the California Current large marine ecosystem. *Science*, **319**, 920, doi:10.1126/science.1149016.

Connolly, T. P., B. M. Hickey, S. L. Geier, and W. P. Cochlan, 2010: Processes influencing seasonal hypoxia in the northern California Current System. *J. Geophys. Res.*, **115**, C03021, doi:10.1029/2009JC005283.

Diaz, R. J., and J. Rosenberg, 1995: Marine benthic hypoxia: A review of its ecological effects and the behavioural responses of benthic macrofauna. *Oceanogr. Mar. Biol.*, **33**, 245–303.

——, and R. Rosenberg, 2008: Spreading dead zones and consequences for marine ecosystems. *Science*, **321**, 926–929, doi:10.1126/science.1156401.

Eriksen, C. C., T. J. Osse, R. D. Light, T. Wen, T. W. Lehman, P. L. Sabin, J. W. Ballard, and A. M. Chiodi, 2001: Seaglider: a long-range autonomous underwater vehicle for oceanographic research. *IEEE J. Oceanic Eng.*, **26**, 424–436, doi:10.1109/48.972073.

Garau, B., S. Ruiz, W. G. Zhang, A. Pascual, E. Heslop, J. Kerfoot, and J. Tintore, 2011: Thermal lag correction on Slocum CTD glider data. *J. Atmos. Oceanic Technol.*, **28**, 1065–1071, doi:10.1175/JTECH-D-10-05030.1.

Garrett, C., P. MacCready, and P. Rhines, 1993: Boundary mixing and arrested Ekman layers: Rotating stratified flow near a sloping boundary. *Annu. Rev. Fluid Mech.*, **25**, 291–323.

Grantham, B. A., F. Chan, K. J. Nielsen, D. S. Fox, J. A. Barth, A. Huyer, J. Lubchenco, and B. A. Menge, 2004: Upwelling-driven nearshore hypoxia signals ecosystem and oceanographic changes in the northeast Pacific. *Nature*, **429**, 749–754, doi:10.1038/nature02605.

Gray, J. S., R. S. Wu, and Y. Y. Or, 2002: Effects of hypoxia and organic enrichment on the marine environment. *Mar. Ecol. Prog. Ser.*, **238**, 249–279, doi:10.3354/meps238249.

Hales, B., L. Karp-Boss, A. Perlin, and P. A. Wheeler, 2006: Oxygen production and carbon sequestration in an upwelling coastal margin. *Global Biogeochem. Cycles*, **20**, GB3001, doi:10.1029/2005GB002517.

Huyer, A., 1976: A comparison of upwelling events in two locations: Oregon and Northwest Africa. *J. Mar. Res.*, **34**, 531–546.

——, E. J. C. Sobey, and R. L. Smith, 1979: The spring transition in currents over the Oregon continental shelf. *J. Geophys. Res.*, **84**, 6995–7011, doi:10.1029/JC084iC11p06995.

——, J. H. Fleischbein, J. Keister, P. M. Kosro, N. Perlin, R. L. Smith, and P. A. Wheeler, 2005: Two coastal upwelling domains in the northern California Current System. *J. Mar. Res.*, **63**, 901–929, doi:10.1357/002224005774464238.

Keller, A. A., V. Simon, F. Chan, W. W. Wakefield, M. E. Clarke, J. A. Barth, D. Kamikawa, and E. L. Fruh, 2010: Demersal fish and invertebrate biomass in relation to an offshore hypoxic zone along the US West Coast. *Fish. Oceanogr.*, **19**, 76–87, doi:10.1111/j.1365-2419.2009.00529.x.

Large, W. G., J. C. McWilliams, and S. C. Doney, 1994: Oceanic vertical mixing: A review and a model with a nonlocal boundary layer parameterization. *Rev. Geophys.*, **32**, 363–403, doi:10.1029/94RG01872.

Lentz, S. J., and D. C. Chapman, 2004: The importance of nonlinear cross-shelf momentum flux during wind-driven coastal upwelling. *J. Phys. Oceanogr.*, **34**, 2444–2457, doi:10.1175/JPO2644.1.

McCabe, R. M., B. M. Hickey, E. D. Dever, and P. MacCready, 2015: Seasonal cross-shelf flow structure, upwelling relaxation, and the along-shelf pressure gradient in the northern California Current System. *J. Phys. Oceanogr.*, **45**, 209–227, doi:10.1175/JPO-D-14-0025.1.

Merckelbach, L. M., R. D. Briggs, D. A. Smeed, and G. Griffiths, 2008: Current measurements from autonomous underwater gliders. *IEEE/OES Ninth Working Conf. on Current Measurement Technology*, Charleston, SC, IEEE, 61–67, doi:10.1109/CCM.2008.4480845.

Nash, J. D., and J. N. Moum, 2001: Internal hydraulic flows on the continental shelf: High drag states over a small bank. *J. Geophys. Res.*, **106**, 4593–4611, doi:10.1029/1999JC000183.

Ordonez, C., 2012: Absolute Water Velocity Profiles from Glider-mounted Acoustic Doppler Current Profilers. M.S. thesis, College of Earth, Ocean and Atmospheric Sciences, Oregon State University, 60 pp.

Pelland, N. A., C. C. Eriksen, and C. M. Lee, 2013: Subthermocline eddies over the Washington continental slope as observed by Seagliders, 2003–09. *J. Phys. Oceanogr.*, **43**, 2025–2053, doi:10.1175/JPO-D-12-086.1.

Perlin, A., J. N. Moum, and J. M. Klymak, 2005: Response of the bottom boundary layer over a sloping shelf to variations in alongshore wind. *J. Geophys. Res.*, **110**, C10S09, doi:10.1029/2004JC002500.

Peterson, J. O., C. A. Morgan, W. T. Peterson, and E. Di Lorenzo, 2013: Seasonal and Interannual variation in the extent of hypoxia in the northern California Current from 1998 – 2012. *Limnol. Oceanogr.*, **58**, 2279–2292, doi:10.4319/lo.2013.58.6.2279.

Pierce, S. P., J. A. Barth, R. E. Thomas, and G. W. Fleischer, 2006: Anomalously warm July 2005 in the northern California Current: Historical context and significance of cumulative wind stress. *Geophys. Res. Lett.*, **33**, L22S04, doi:10.1029/2006GL027149.

——, ——, R. K. Shearman, and A. Y. Erofeev, 2012: Declining oxygen in the northeast Pacific. *J. Phys. Oceanogr.*, **42**, 495–501, doi:10.1175/JPO-D-11-0170.1.

Reid, J. L., and A. W. Mantyla, 1976: The effect of the geostrophic flow upon coastal sea elevations in the northern North Pacific Ocean. *J. Geophys. Res.*, **81**, 3100–3110, doi:10.1029/JC081i018p03100.

Rudnick, D. L., and S. T. Cole, 2011: On sampling the ocean using underwater gliders. *J. Geophys. Res.*, **116**, C08010, doi:10.1029/2010JC006849.

Smith, R. L., 1981: A comparison of the structure and variability of the flow field in three coastal upwelling regions: Oregon, northwest Africa, and Peru. *Coastal Upwelling*, F. A. Richards, Ed., Coastal Estuarine Sciences Series, Vol. 1, Amer. Geophys. Union, 107–118, doi:10.1029/CO001p0107.

Suanda, S. H., and J. A. Barth, 2015: Semidiurnal baroclinic tides on the central Oregon inner shelf. *J. Phys. Oceanogr.*, **45**, 2640–2659, doi:10.1175/JPO-D-14-0198.1.

Todd, R. E., D. L. Rudnick, and R. E. Davis, 2009: Monitoring the greater San Pedro Bay region using autonomous underwater gliders during fall of 2006. *J. Geophys. Res.*, **114**, C06001, doi:10.1029/2008JC005086.

——, ——, M. R. Mazloff, R. E. Davis, and B. D. Cornuelle, 2011: Poleward flows in the southern California Current System: Glider observations and numerical simulation. *J. Geophys. Res.*, **116**, C02026, doi:10.1029/2010JC006536.